Acta Aquatica Turcica
E-ISSN: 2651-5474
Home Page: https://dergipark.org.tr/actaquatr 20(3): 218-241, 2024 DOI: 10.22392/actaquatr.1418335
Research Article Araştırma Makalesi

Design, Development and Performance Evaluation of a Motorized Periwinkle Meat Extraction Machine

Motorlu Deniz Salyangozu Et Ekstraksiyon Makinesinin Tasarımı, Geliştirilmesi ve Performans Değerlendirmesi

Inemesit Ekop[1,*], Joseph Bassey[2], Ifiok Ekop[3], Promise Etim[1], Godwin Akpan[1], Ololade Olatunji[1], Paul Tosin[4], Kayode Simonyan[4], Udochukwu Onwuka[4]

[1]Department of Agricultural Engineering, Faculty of Engineering, Akwa Ibom State University, Ikot Akpaden, P.M.B. 1167, Uyo, Akwa Ibom State-NIGERIA
[2]Department of Mechanical Engineering, Faculty of Engineering, Akwa Ibom State University, Ikot Akpaden, P.M.B. 1167, Uyo, Akwa Ibom State-NIGERIA
[3]Department of Building, Faculty of Environmental Studies, University of Uyo. P.M.B. 1017, Uyo, Akwa Ibom State-NIGERIA
[4]Department of Agricultural and Bioresources Engineering, College of Engineering and Engineering Technology, Michael Okpara University of Agriculture, Umudike, P.M.B 7262, Umuahia, Abia State-NIGERIA

*Corresponding Author: inemesitekop@aksu.edu.ng

Received: 15. 01.2024 **Accepted:** 22.04.2024 **Published:** 01.09.2024

How to Cite: Ekop, I., Bassey, J., Ekop, I. , Etim, P. , Akpan, G. , Olatunji, O. , Tosin, P. , Simonyan, K. & Onwuka, U. (2024). Design, development and performance evaluation of a motorized periwinkle meat extraction machine. *Acta Aquatica Turcica, 20*(3), 218-241. https://doi.org/10.22392/actaquatr.1418335

Abstract: Efficient cracking and separation of periwinkle shells are essential unit operations in periwinkle meat processing. Mechanization remains the panacea to achieving timely processing of periwinkle meat. This study was carried out to design, develop, and evaluate the performance of a viable machine for the extraction of meat from periwinkle. The performance of the machine was dependent on certain processing parameters, such as cracking speed (*CS*), Agitating speed (*AS*), feed rate (*FR*) and heat conditioning time (*HCT*), while periwinkle cracking efficiency (*CE*), separating efficiency (*SE*), Throughput capacity (*TP*) and periwinkle meat loss (*PML*) were the responses. The maximum periwinkle meat *CE* of 84.05 % was obtained at CS of 130 rpm, FR of 0.2 kgs^{-1} and HCT of 6 min. The result for *SE* indicated that most efficient periwinkle meat separation of 78.79% can be achieved when *HCT*, *CS*, *AS* and *FR* set at 6 min,130 rpm,1.11m/s and 0.40 kg/s respectively. Highest *TP* value of 26.79 kg/h was obtained when the machine was operated at *CS* of 130 rpm, *AS* of 1.23 m/s under the *HCT* of 6 min at *FR* of 0.40 kg/s. Also, the lowest *PML* value of 10.71 % was obtained when the machine was operated at *CS* of 120 rpm, *AS* of 1.04 m/s under the *HCT* of 4 min at feed rate of 0.30 kg/s. These machine parameters have significant effects on the periwinkle meat processing. The study has provided a viable option to replace the time-consuming, crude manual method of periwinkle meat postharvest processing.

Keywords
- Periwinkle meat
- Extraction
- Design
- Development
- Performance evaluation

Özet: Deniz salyangozu kabuklarının verimli bir şekilde parçalanması ve ayrılması, deniz salyangozu eti işlemede temel birim işlemlerdir. Mekanizasyon, deniz salyangozu etinin zamanında işlenmesini sağlamak için her derde deva olmaya devam ediyor. Bu çalışma, deniz salyangozundan et ekstraksiyonu için uygun bir makinenin tasarımını yapmak, geliştirmek ve performansını değerlendirmek için yapılmıştır. Makinenin performansı, çatlama hızı (CS), Çalkalama hızı (AS), ilerleme hızı (FR) ve ısı şartlandırma süresi (HCT) gibi belirli işleme parametrelerine bağlıyken, deniz salyangozu kırma verimliliği (CE), ayırma verimliliği (SE), Verim kapasitesi (TP) ve deniz salyangozu et kaybı (PML) yanıtlardı. Maksimum deniz salyangozu eti %84.05 CE, 130 rpm CS, 0.2 kgs-1 FR ve 6 dakika HCT'de elde edildi. SE için elde edilen sonuç, HCT, CS, AS ve FR sırasıyla 6 dk, 130 rpm, 1,11 m/s ve 0,40 kg/s'ye ayarlandığında %78,79'luk en verimli deniz salyangozu eti ayrımının elde edilebileceğini gösterdi. 26,79 kg/s ile en yüksek TP değeri, makine 130 rpm'lik CS'de, 0,40 kg/s'lik FR'de 6 dakikalık HCT altında 1,23 m/s'lik AS'de çalıştırıldığında elde edildi. Ayrıca, %10,71'lik en düşük PML değeri, makine 120 rpm'lik CS'de, 0,30 kg/s'lik ilerleme hızında 4 dakikalık HCT altında 1,04 m/s'lik AS'de çalıştırıldığında

Anahtar kelimeler
- Deniz salyangozu eti
- Çıkarma
- Tasarım
- Gelişme
- Performans değerlendirme

elde edilmiştir. Bu makine parametrelerinin deniz salyangozu eti işleme üzerinde önemli etkileri vardır. Çalışma, deniz salyangozu etinin hasat sonrası işlenmesinin zaman alıcı, ham manuel yönteminin yerini almak için uygun bir seçenek sağlamıştır.

1. INTRODUCTION

Periwinkle meat contains high-quality proteins, minerals such as calcium, potassium, iron, and phosphorus, as well as vitamins. It includes sufficient amounts of the most important amino acids for human nutrition. The periwinkle shells are possible sources of calcium for animal feeds (Ekop et al., 2019). In most producing places in Nigeria, there is no information on the annual harvest or output of periwinkle. A recent survey of some riverine communities in Itu, Oron, Issiet, Okobo, and Uta-ewa in Akwa Ibom State shows an abundance of periwinkle, with over 10 tons harvested annually. Thirty-five mangrove villages in Nigeria's Delta and Rivers States harvest roughly 40.3 tons of periwinkle each year. Some localities in Nigeria's Bayelsa, Cross River, and Edo states have reported large scale periwinkle output (Ekop et al., 2021; Mmom & Arokoyu, 2010; Jamabo & Chinda, 2010).

Over the years, the processing of periwinkle has been carried out through traditional manual methods, which involve using a knife to trim the tapered end and cooking it with its shell after thorough washing. The process includes immersing it in hot water until it froths (flash pasteurization) and then using a sterile needle to extract the meat from its shell (Odu et al., 2010). This makes the processing of periwinkle tedious, time consuming, unwholesome, and uneconomical. Additionally, the shape, size, varieties, and other physiological factors further make the development of efficient processing of periwinkle difficult, thereby limiting its economic potential. Considering the processing challenges associated with the crude manual method of processing periwinkle, this work focused on developing an efficient mechanize system for periwinkle meat processing.

2. MATERIALS AND METHODS

2.1. Design considerations for periwinkle meat processing machine

For hygienic and safe processing of periwinkle meat, the following design criteria were considered:

i. Material selection was done in conformity to salubrious design principles, periwinkle meat contact surfaces were made with materials that are plane, easy to clean, non-toxic, non-corrosive, and inert to periwinkle meat and cleaning agent.

ii. Design related to the physical, mechanical and thermal characteristics of the machine were made using appropriate standards (i.e., according to the American Society of Mechanical Engineering (ASME) standard) and were also based on the computed theoretical analysis.

iii. Raw materials used were locally sourced for the construction of the machine.

iv. Minimal power requirement was targeted; hence, a 2.5 HP electric motor was adopted to run the machine.

v. The operation and maintenance of the machine were made simple with friendly user-interface.

2.2. Design concept

The periwinkle meat processing machine comprised of the following:

(i) Feed hopper to receive the periwinkle into the machine.

(ii) Two cylindrical cracking rollers for cracking the periwinkle shell to obtain the meat.

(iii) Transmission unit; which is the machine's prime mover.

(iv) The separating and cleaning units for actual sorting and separating periwinkle meats from the shells.

2.3. Design analysis and calculations of machine components

Several analysis and calculations were made based on the results of the measured engineering properties of the periwinkle.

2.4. Design of the hopper

The hopper is the receptacle through which periwinkle is admitted into the machine for cracking. It has a composition of a trapezium and rectangle cross-section made with stainless steel sheet. Figure 1 (a) and (b) show the assembly and exploded view of the hopper respectively.

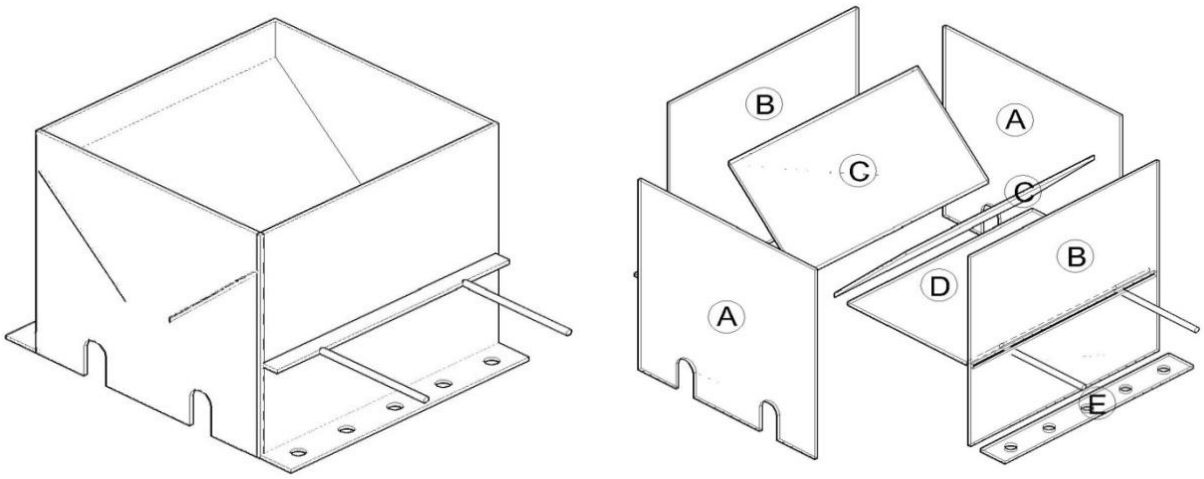

(a) Assembly drawing (b) Exploded drawing

Figure 1. Assembly drawing (a) and exploded drawing (b) of the hopper.

The cross-sectional area was determined according to Otto (2015) as

$S_A = (a \times b)$ (1)

where, S_A= rectangular section surface area (m^2), a = rectangular length (m),

b = rectangular width (m)

$S_A = (0.3 \times 0.316) = 0.0948\ m^2$

A 20-gauge stainless steel sheet of 800×470 mm, with thickness of 1.0058 mm was used to construct and form the hopper of the machine.

Capacity of the hopper C_{aH}, is expressed as

C_{aH} = (cross-sectional area) × (hopper's length) (2)

$$C_{aH} = 0.0948\ m^2 \times 0.312\ m = 0.0296\ m^3$$

2.5. Design of the outlet chute

The outlet chute constitutes the discharge chamber that expels the cracked periwinkles into the separating unit. It has a trapezoidal shape made with stainless sheet. Figure 2 shows the assembly and exploded drawings of the outlet chute.

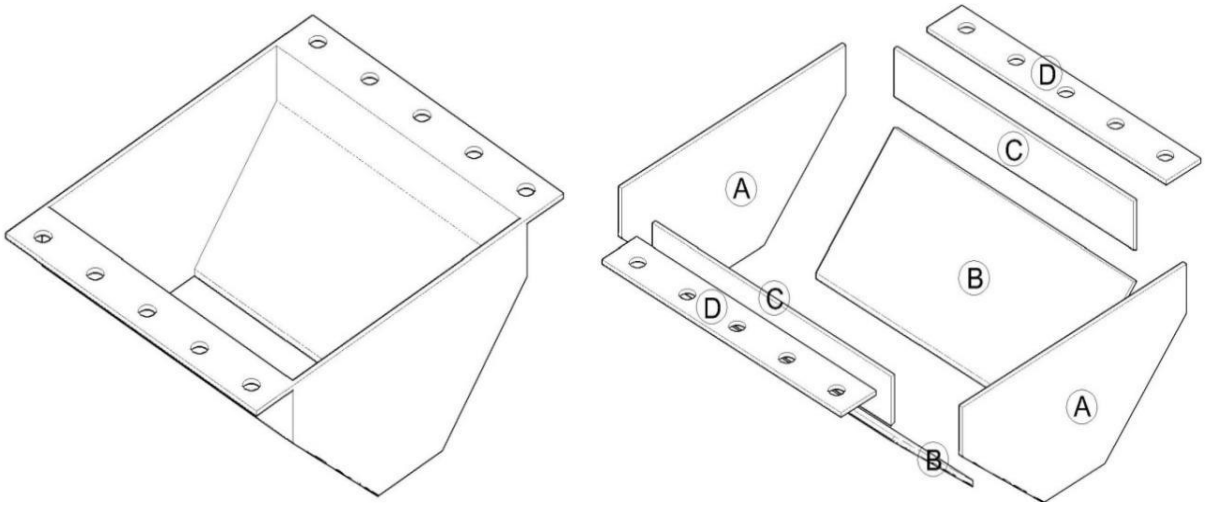

(a) Assembly drawing (b) Exploded drawing

Figure 2. Assembly drawing (a) and exploded drawing (b) of the outlet chute.

The cross-sectional area of the outlet chute as stated by Otto (2015) is expressed as

$S_{A1} = L \times B$ (3)

where, S_{A1} = rectangular section surface area (m^2), L= rectangular length (m),
B = rectangular width (m), and

$$S_{A2} = \frac{1}{2}(a+b)h \quad (4)$$

where, S_{A2} = trapezoidal section surface area (m^2), a = rectangular length (m),
b = rectangular width (m) h = trapezoidal height (m).

The outlet chute cross-sectional area (S_{A2}) was computed as $0.0332\ m^2$.

A 20-gauge stainless steel sheet of $450 \times 510\ mm$, with thickness of $1.0058\ mm$ was used to construct the outlet chute of the machine.

Hence, the capacity of the outlet chute (C_{aOC}) is given by

C_{aOC} = (cross-section area) × (length of the hopper outlet chute) (5)

$$C_{aOC} = 0.0104\ m^3$$

2.6. Design of the cracking unit

The cracking unit consists of two identical cylindrical rollers which were prepared using hollow cylindrical mild Steel of $350\ mm \times 138\ mm$ by cutting and welding it into actual dimensions as shown in Figure 3. The final surfaces of the cylindrical roller were knurled for better friction.

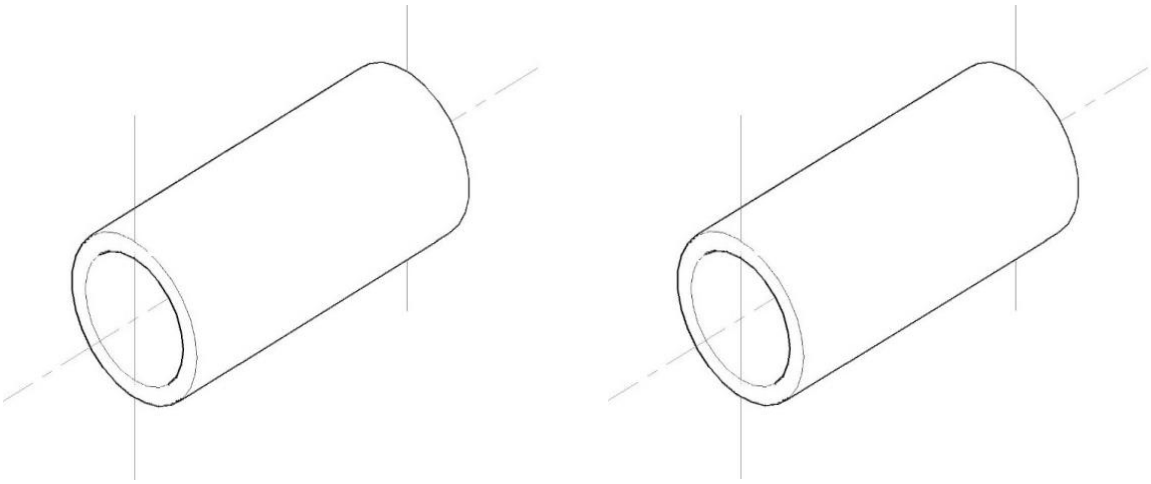

Figure 3. Hollow cylinders for the cracking rollers.

Mass of hollow cylinder material for periwinkle cracking roller was determined using expression given by Otto (2015) as

$$Mass, m_{HC} = \rho v \quad (6)$$

where, m_{HC} = mass of the material used for the cracking roller (kg)
ρ = density of mild Steel sheet = 7850 kgm^{-3} (Umani et al., 2019)
v = volume of the cracking roller (m^3)
Surface area of the cracking roller in m^2, as given by Otto (2015) is expressed as:

$$S_{HC} = 2\pi R \times L \quad (7)$$

where, S_{HC} = surface area of the hollow cylinder (m^2)
R = external radius of the hollow cylinder (m)
L = length of the hollow cylinder (m)

$$S_{HC} = 2\pi R \times L = 0.1517\ m^2$$

But, V = cracking surface area (m^2) × thickness of the material used (m)
$= 0.002276\ m^3$ and, $Mass, m_{HC} = 17.87\ kg$
Thus, Mass of circular disc material for cracking roller as given by Otto (2015).

$$Mass, m_C = \rho v' \quad (8)$$

where, m_C = mass of circular disc material for cracking roller (kg)
ρ = density of mild Steel sheet = 7850 kgm^{-3} (Umani et al., 2019)
v' = volume of the cracking roller (m^3)
Surface area of the cracking roller in m^2 as given by Otto (2015) is expressed as

$$v' = \pi r^2 \mathrm{t} \quad (9)$$

where, r = radius of the disc material (m), and t = thickness of the disc material (m).

$$v' = \pi(0.069)^2 \times 0.015 = 0.000224\ m^2$$

Thus, $Mass, m_C = \rho v' = 7850\ kgm^{-3} \times 0.000224\ m^3 = 1.76\ kg$

Therefore, the mass for covering the hollow cylinder opening is given by

$$m_C = 1.76 \times 2 = 3.52\ kg$$

Mass of the cracking roller, m_{CR} is given as

m_{CR} = (mass of hollow cylinder material for periwinkle cracking rollers $(m_{HC})) +$ (mass for covering the hollow cylinder opening(m_C))

Thus, $m_{CR} = (17.87 + 3.52) = 21.39kg$

The periwinkle cracking unit mechanism is shown below in Figure 4.

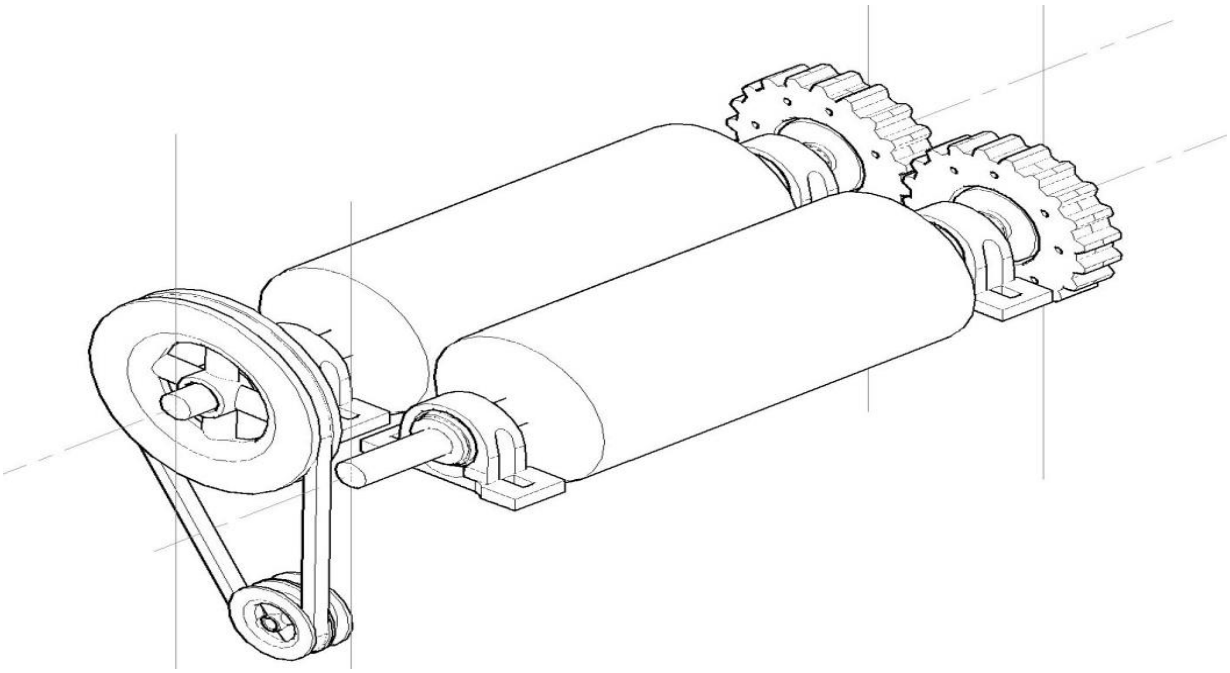

Figure 4. An isometric view of the cracking unit.

2.7. Power requirements to crack periwinkle

In order to determine the power required to efficiently crack periwinkle, it is essential to establish the different forces acting on the cracking rollers. These forces are: (i) force due to periwinkle dropping on the surface of the rollers (ii) average compression force that is required to crack periwinkle (iii) frictional compression force required to crack periwinkle; and, (iv) rotational torque required on the periwinkle cracking rollers.

(i) Force due to periwinkle dropping (F_{pd})

The dropping effect of the periwinkle from the hopper inlet to the rotating surface has a force effect greater than the weight of the periwinkle. Since the Potential Energy of the periwinkle can be expressed as mhg and its Kinetic Energy at impact is $\frac{mv^2}{2}$, where, h = height of object in meters, m = mass of object in kg, g = acceleration due to gravity (9.81 m/s^2), v = velocity at impact in m/s.

Hence, $h = \frac{v^2}{2}$, and $v = \sqrt{2gh}$

Since the dropping force (F_{pd}) can be expressed as shown in equation 10

$$F_{pd} = ma = m\left(\frac{v-u}{t}\right) \quad (10)$$

where, u = velocity of periwinkle before impact (here, it is assumed to be zero (0)

v =velocity at impact,

t = time in seconds (here, time of impact is assumed to be 1 second)

hence, dropping force, $F_{pd} = m\left(\frac{v-0}{1}\right) = m(\sqrt{2gh})$ (10a)

Since, m = mass of a periwinkle (kg) = 4.4g = 0.0044kg (measured), g = acceleration due to gravity (ms^{-2}) = 9.81 ms^{-2}, h = height from hopper inlet discharge chute to the roller surface (m) = 0.066 m (measured).

$$F_{pd} = 0.0044 \times (\sqrt{2 \times 9.81 \times 0.066}) = 0.005\ N$$

Maximum allowable number of periwinkles dropping per unit time in seconds is twenty (20) periwinkles. This was based on the opening of the inlet control. Thus, Maximum periwinkle dropping force per unit second is

$$F_{pd} = 0.005 \times 20 = 0.1\ N$$

(ii) Average compression force that is required to crack a single periwinkle is denoted as F_c. From experiment, this force is measured and has a magnitude of 746.1 *N* (Ekop et al., 2022).

(iii) Frictional compressive force induced between the roller surface and the loaded periwinkle during the cracking process is denoted as F_{fc}. This force may also be expressed as

$$F_{fc} = \mu N \quad (11)$$

where, μ = friction coefficient between the roller surface and periwinkle, *N* = normal reaction force,

Since the average compressive force is the force the roller must overcome to crack a single periwinkle, thus we can say that *N* is equal to F_c. Hence

$$F_{fc} = \mu N = \mu F_c \quad (11a)$$

Taking μ to be 0.9 (i.e., maximum possible frictional resistance),

$$F_{fc} = 0.9 \times 846 = 761.4\ N$$

(iv) The torque required to be developed to crack a periwinkle may be expressed as

$$T = F_{fc} \times r \quad (12)$$

Where r = radius of rotation (radius of cracking roller = 0.069 m)

$$T = 761.4 \times 0.069 = 52.54\ Nm$$

The power required (P_R) to be developed to crack a periwinkle may be expressed a

$$P_R = T\omega = (T) \times \frac{2\pi N}{60} \quad (13)$$

where, *N* is the speed of the cracking roller (the maximum speed of the cracking roller was set at 160 rpm.) (Ekop et al., 2022).

Thus, $$P_R = 52.54 \times \frac{2 \times \pi \times 160}{60} = 52.54 \times 16.76 = 880.6\ Watt$$

From the design of the machine, two cracking rollers are used. Thus, the cracking force developed by a single roller may be expressed as

$$F_{rc} = ma = m_{GD}\omega^2 r \quad (14)$$

where, m_{GD} = mass of periwinkle cracking roller = 21.39 kg

r = radius of rotation (radius of cracking roller = 0.069 m)

ω = angular velocity of the cracking roller in rad/sec = $\frac{2\pi N}{60}$, and

N = rotational speed of the cracking roller in rpm = 160 rpm

Since two rollers are used, total roller cracking force is equal to

$$F_{rcT} = n_r m_{GD}\omega^2 r \quad (15)$$

where, n_r = number of rollers = 2

Hence, $F_{rcT} = 2 \times 21.39 \times (\frac{2 \times \pi \times 160}{60})^2 \times 0.069 = 829$ N

The torque developed by the rollers, T_r is expressed as

$$T_r = F_{rcT} \times r \quad (16)$$

$$T_r = 829 \times 0.069 = 57.20 Nm$$

Power developed by the machine, P_D to crack a periwinkle may be expressed as

$$P_D = T_r \times \omega \quad (17)$$

$$P_D = 57.20 \times \frac{2 \times \pi \times 160}{60} = 25.2 \times 16.76 = 958.72\ Watt$$

Machine Power ratio, M_{PR} may be expressed as

$$M_{PR} = \frac{P_D}{P_R} \quad (20)$$

$$M_{PR} = \frac{958.72}{880.6} = 1.1$$

Thus, this means that the machine power safety factor is 1.1 times the required power to crack a single periwinkle.

2.8. Selection of electric motor and transmission drive

The machine was design and rated at 1.875kW (i.e., 2.5 hp). This allowed the machine to conveniently crack two (2) periwinkles per second (i.e., $\frac{2.5\times746}{880.6} = 2.12 \approx 2$) and still have additional power to drive the system auxiliaries (e.g., cams, belt and gears system). However, an electric motor having the following rated specification was selected to provide for total power requirement in the system.

Power, P = 2.24 kW (3.0 HP)
Rotational Speed, N = 1440 rpm
Frequency = 50 Hz
Phase = 3

The machine's power transmission drives were pulleys and belts.

2.9. Selection of transmission system

A pulley system with open belt as shown in Figure 5 was used to transfer motion from the driving shaft (electric motor shaft) to the roller shaft.

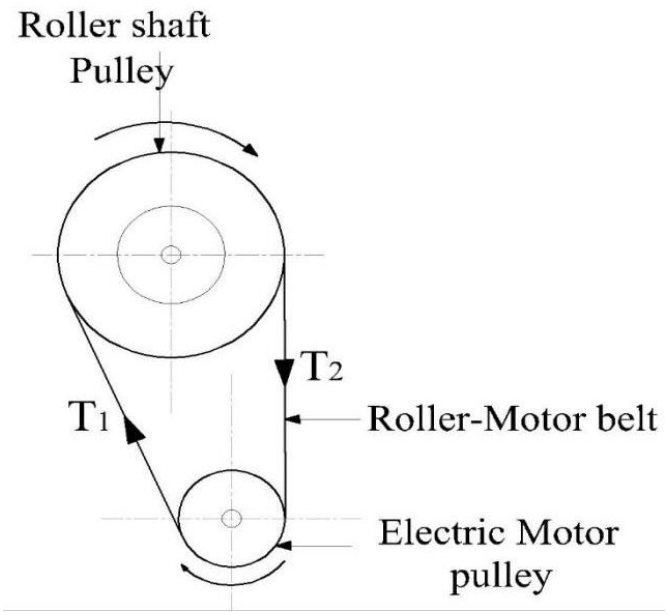

Figure 5. Pulley and open belt drive system.

The electric motor speed is 1400 rpm, this speed can be varied with the help of a regulator switch. The maximum speed of the driven pulley was determined from the velocity ratio expression given by Khurmi & Gupta (2008) and Hicks (2004) as

$$\frac{N_1}{N_2} = \frac{D_2}{D_1} \quad (21)$$

where, N_2 = speed of roller 1 shaft in rpm
N_1 = speed of electric motor shaft in rpm
D_2 = roller 1 shaft pulley diameter in mm (= 153mm = 0.153m)
D_1 = electric motor pulley diameter in mm (= 74mm= 0.074m)
Thus, the speed ratio of the system was calculated as: ($\frac{D_2}{D_1} = \frac{0.153}{0.074}$) = 2.1

2.10. Determination of the length of belt (L_b)

Power is transmitted from the electric motor pulley to the cracking rollers through the belt drive. The pulley used has a V-slot, hence a V-belt type was used. A sizeable belt length was selected according to the relation expressed by Khurmi & Gupta (2008) as

$$L_b = \frac{\pi}{2}(D_2 + D_1) + 2C + \frac{(D_2 - D_1)^2}{4C} \quad (22)$$

where, L_b= length of belt in mm, C = centre distance of pulleys

D_1 and D_2 = effective or pitch diameter (mm) of smaller and larger pulleys respectively.

Thus, $$C = \left(\frac{D_2}{2} + \frac{D_1}{2}\right) + D_1 \quad (23)$$

$$C = \left(\frac{153}{2} + \frac{74}{2}\right) + 74 = 261.5\, mm$$

Hence, substituting 261.5mm for C in equation 22, we have

$$L_b = \frac{\pi}{2}(153 + 74) + 2(261.5) + \frac{(153 - 74)^2}{4(261.5)} = 885.54\, mm$$

2.11. Determination of belt speed V_{bs}

The speed of the belt was determined as described in V-Belt Design Manual, (2017) as

$$V_{bs} = \frac{\pi N_1 D_1}{60} \quad (24)$$

where, V_{bs} = peripheral velocity of the belt in m/s, N_1 = speed of the electric motor in rpm

D_1 = pulley diameter of the electric motor in mm.

Hence, $$V_{bs} = \frac{\pi \times 1440 \times 0.074}{60} = 5.58 ms^{-1}$$

2.12. Angle of contact of roller-1/motor pulleys

Considering an open belt, the lap angle of the belt according to Khurmi and Gupta (2008), was determined using equations 25 and 26.

$$\theta = \left(180 - 2(\propto)\frac{\pi}{180}\right) rad \quad (25)$$

$$\propto = sin^{-1}\left[\frac{D_2 - D_1}{2C}\right] \quad (26)$$

where, C = centre distance of the pulleys $in\ mm$

D_1 = pulley diameter of the prime mover, mm

D_2 = pulley diameter of roller 1 shaft (driven), mm

$\propto$ = joint angle (°)

Hence, $$\propto = sin^{-1}\left[\frac{153 - 74}{2 \times 261.5}\right] = 8.69°$$

$$\theta = [180 - 2(8.69)\left(\frac{\pi}{180}\right)]$$

$$\theta = 162.62 \times \left(\frac{\pi}{180}\right)$$

$$= 2.84\, rad$$

2.13. Friction coefficient between the belt and roller-1/motor pulley

Khurmi and Gupta (2008) reported that the coefficient of friction (μ) for leather belts on cast iron pulleys, at the point of slipping is given by the relation in equation 27

$$\mu = 0.54 - \left[\frac{42.5}{152.6 + v}\right] \quad (27)$$

where, v = speed of belt, $m\ min^{-1} = 5.58\, ms^{-1} = 5.58 \times 60 = 334.8\, m\ min^{-1}$

$$\mu = 0.54 - \left[\frac{42.5}{152.6 + 334.8}\right] = 0.45$$

2.14. Determination of tension (T_1 and T_2) on roller-1/motor belt

According to Khurmi and Gupta (2008), the tension on the tight side of the belt is given in equation 28 as

$$P = (T_1 - T_2)V_{bs} \quad (28)$$

where, T_1 = tension in the tight side of the belt in N

T_2 = tension in the slack side of the belt in N

P = power transmitted from electric motor = 2.5 HP = 1.875 kW

V_{bs} = belt speed ($5.58 ms^{-1}$)

For a V-belt drive, the tension ratio can be expressed as Khurmi and Gupta (2008)

$2.3\log(\frac{T_1}{T_2}) = \mu\theta$ (29)

$2.3\log(\frac{T_1}{T_2}) = 0.45 \times 2.84$

Solving equations 28 and 29 simultaneously yielded

$$T_1 = 465.26\ N, and\ T_2 = 129.24\ N$$

2.15. Cross-sectional area (a_b) of the V-belt

The area of cross-section of the V-belt was determined by considering the areas A, B, and C in Figure 6. From Table 1, the top width (b) and the thickness (t) of the A-type V-belt are 13 and 8 mm respectively, therefore the cross-sectional area of the V-belt was determined using equation 30.

Area of belt (a_b) = area of triangles (A + B + C).

$a_b = \left[\frac{1}{2}\left(\frac{b-a}{2}\right)t + at + \frac{1}{2}\left(\frac{b-a}{2}\right)t\right]$ (30)

Where, b= top width of the belt = 13 mm; a = base width of the belt = ? ;

t = thickness of the belt = 8 mm

From Figure 6, the groove angle for A-type V-belt is given as:

$2\beta = 34^o$ and $\beta = 17^o$ (Khurmi & Gupta 2008)

Note: $\mu =$ friction coefficient between the belt and pulley = 0.44;

θ = lap angle of the belt on roller 1-motor pulley = 3.14 rad; and

β = groove angle of the pulley = 17°

From Figure 6, $x = \frac{b-a}{2}$ (31)

But, $x = t\ tan\ 17^0 = 8\ tan\ 17^0 = 2.45\ mm$

From equation 31, $a = 13 - 2(2.45) = 8.1\ mm$

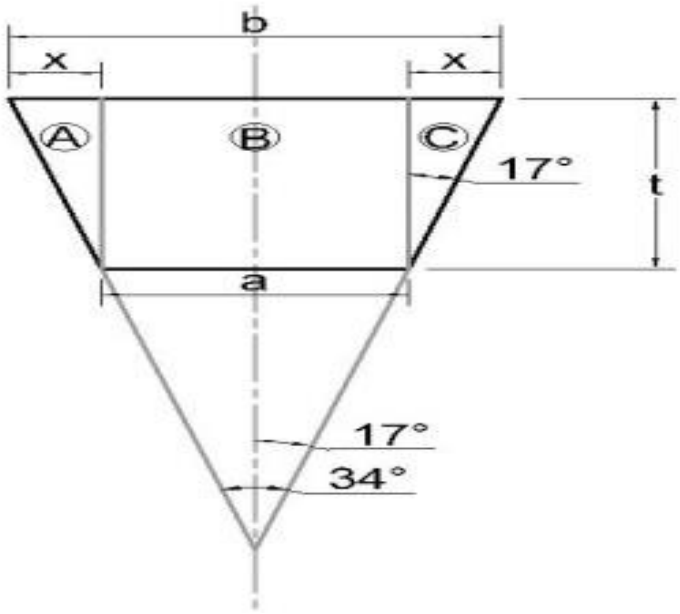

Figure 6. Cross-section of V-belt for roller-1 transmission drive.

Substituting the values 13, 8.1 and 8mm for b, a and t respectively into equation 30, we have

$$a_b = \left[\frac{1}{2}\left(\frac{13-8.1}{2}\right)8 + 8.1(8) + \frac{1}{2}\left(\frac{13-8.1}{2}\right)8\right] mm^2$$

$= 84.4\ mm^2 = 0.0000844\ m^2$

Table 1. Dimensions of standard V-belts.

Types of belt	Power range in kW	Minimum-pitch diameter of pulley (D) mm	Top Width (b) mm	Thickness (t) mm	Weight per-meter Length (N)
A	0.7-3.7	75	13	8	1.06
B	2-15	125	17	11	1.89
C	7.5-75	200	22	14	3.43
D	20-150	355	32	19	5.96
E	30-350	500	38	23	---

Source: Khurmi & Gupta 2008.

2.16. Design of shaft

2.16.1 Design for roller-1 shaft

The roller-1 shaft was designed to withstand combined bending and twisting moments. Figure 7 shows loads, forces, and reactions on the roller-1 shaft. The machine elements that exert forces on roller-1 shaft is the belt, pulley (driven pulley), cracking roller, and gear. The shaft with forces acting on it is represented schematically, as shown in Figure 8.

The forces acting on the roller-1 shaft were of vertical and horizontal components. The forces acting on the roller-1 shaft are due to compression force by the cracking roller, force due to periwinkles dropping, weight of the cracking roller, weight of the drive pulley, and tensions in the drive belt.

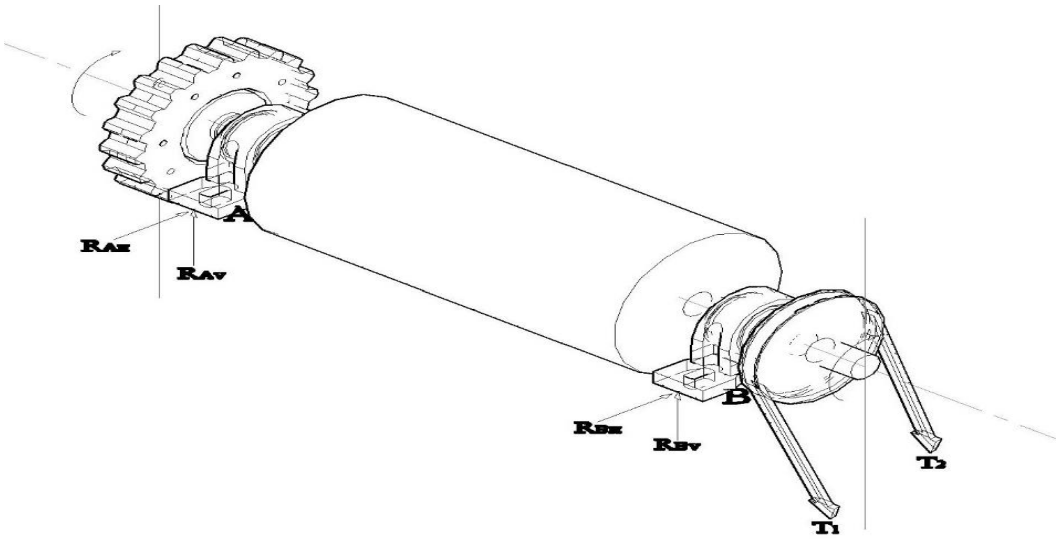

Figure 7. Roller-1 main shaft carrying the periwinkle cracking roller with a pulley, two bearings (A and B) and a gear.

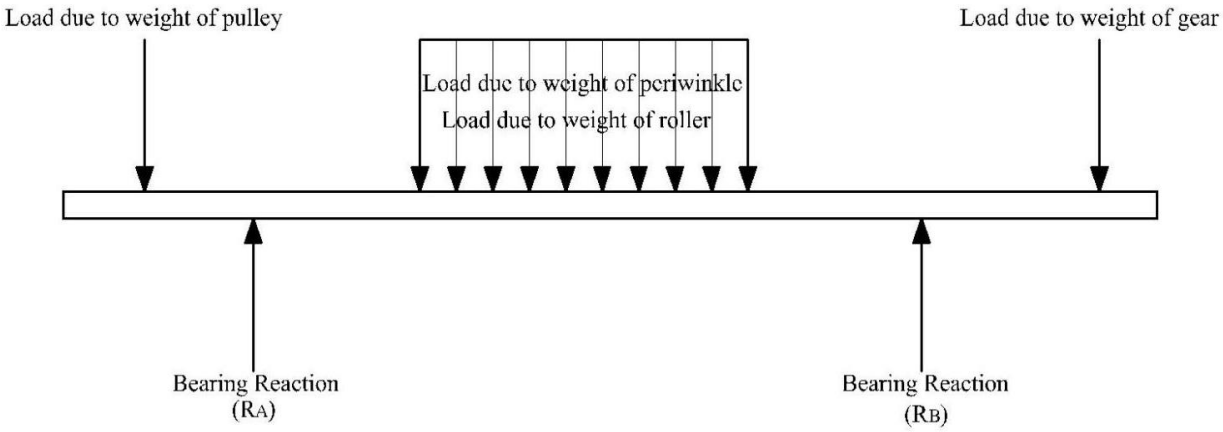

Figure 8. Forces acting on the drive shaft with bearing reaction.

2.16.2. Vertical forces exerted on roller-1 shaft (F_v)

The vertical forces acting on the roller-1 shaft is shown schematically in Figure 9.

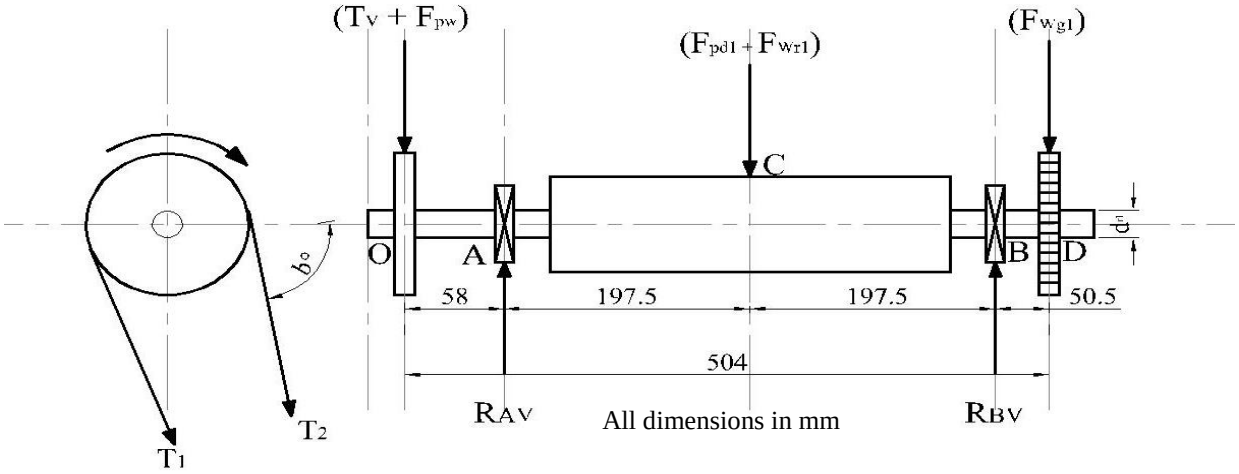

Figure 9. A schematic diagram illustrating the vertical forces acting on the roller-1 shaft.

2.16.3. Force due to periwinkles dropping (F_{pd})

As already computed under the power requirements section, the periwinkle dropping force due to gravity is $(F_{pd}) = 0.1N$

2.16.4. Force due to weight of the cracking roller (F_{wr1})

The force F_{wr1} due to the weight of the cracking roller was determined using the expression given in equation 32, as expressed by Khurmi and Gupta (2008).

$F_{wr1} = M_{CR} \times g$ (32)

Where; M_{CR}= mass of the cracking roller, kg = 21.39kg; g = acceleration due to gravity, ms^{-2}= 9.81 ms^{-2}

$$F_{wr1} = M_{CR} \times g = 21.39 \times 9.81 = 209.84\ N$$

2.16.5. Force due to weight of the drive pulleys (F_{pw})

The force F_{PW} due to the weight of the drive pulleys was determined using the expression given in equation 33, as expressed by Khurmi and Gupta (2008).

$F_{PW} = M_{PU} \times g$ (33)

where M_{PU} = mass of the pulley on roller-1 shaft, kg = 0.897 kg (measured);

g= acceleration due to gravity, ms^{-2}= 9.81 ms^{-2}

$$F_{PW} = M_{PU} \times g = 0.897 \times 9.81 = 8.80\ N$$

2.16.6. Vertical components of tensions in the belt drive (T_v)

$$T_{(1,2)V} = (T_1 + T_2) sin\, b^0 = (465.26 + 129.24) sin\, 78^0$$

$= 581.51\ N$ (force acting downward)

2.16.7. Force due to weight of the gear (F_{wg1})

Force acting tangential to the gear (F_T) was computed using equation proposed by Khurmi and Gupta (2008)

$F_T = 2\frac{T_r}{D}$ (34)

where, D = diameter of the gear ≈ diameter of the roller = 0.138m

$T_r =$ Torque on the cracking roller-1, and

$$T_r = 57.2\ Nm$$

Hence,

$$F_T = 2\frac{T_r}{D} = 2 \times \frac{57.2}{0.138} = 829\ N$$

Normal load acting on the tooth of the gear (F_N) $= \frac{F_T}{\cos\varphi} = 829/\cos 20^0 = 882.2\ N$

φ= pressure angle of the gear taken as 20^0 (Collins et al., 2010)

Vertical Component i.e., load on the shaft due to weight of gear (F_{Wg1}) $= F_N \cos 20^0$

$= 882.2 \times \cos 20^0 = 829\ N$

2.16.7. Summation of the vertical forces exerted on roller-1 shaft

$$F_V = F_{pd} + F_{wr1} + F_{pw} + F_{wg1} + T_v$$
$$= 0.1N + 209.84 + 8.80 + 829 + 581.51$$
$$= 1629.25\ N$$

2.16.8. Horizontal forces exerted on roller-1 shaft (F_h)

The horizontal forces acting on the roller-1 shaft is shown schematically in Figure 10.

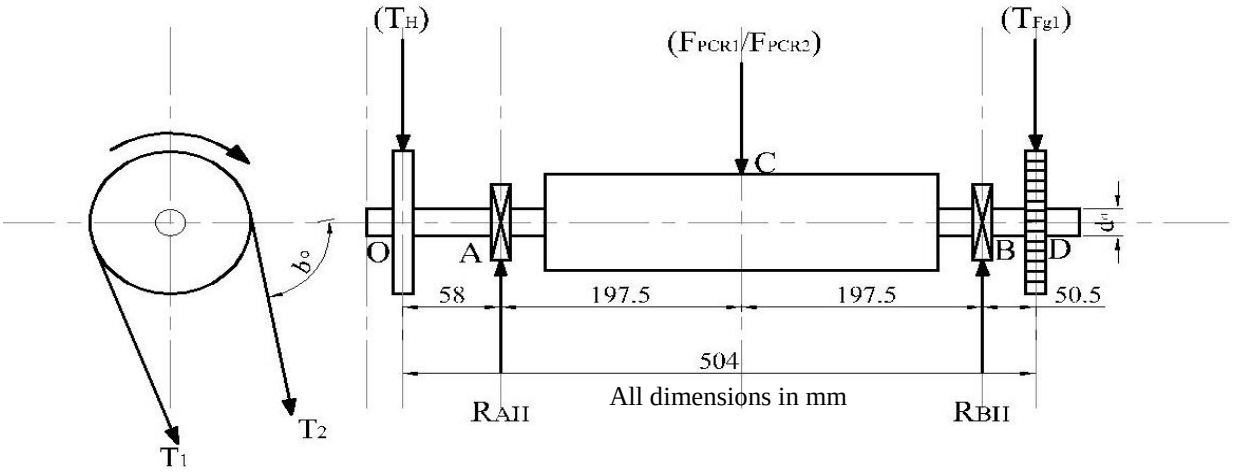

Figure 10. A schematic diagram illustrating the horizontal forces acting on the roller-1 shaft.

2.16.9. Horizontal components of tensions in the belt drive (T_H)

$$T_{(1,2)H} = (T_1 + T_2)cos\ b^0 = (465.26 + 129.24)cos\ 78^0$$

$= 123.6N$ (force acting to the right)

2.16.10. Maximum periwinkle transverse compression force between roller 1 and 2 ($F_{PCR1,2}$)

$F_{PCR1,2} = 746.1\ N$ (measured)

2.16.11. Horizontal component load acting on shaft due to gear torque (F_{pg1})

$F_{pg1} = F_N \sin 20^0 = 882.2 \times \sin 20^0 = 301.7\ N$

2.16.12. Summation of the horizontal forces exerted on the roller-1 shaft

$$F_H = F_{PCR1,2} + F_{pg1} + T_H$$
$$= 746.1 + 301.7 + 123.6$$
$$= 1171.4\ N$$

2.16.13. Reactions at the bearings due to vertical loading

The reactions on roller-1 shaft due to vertical loading is shown in Figure 11.

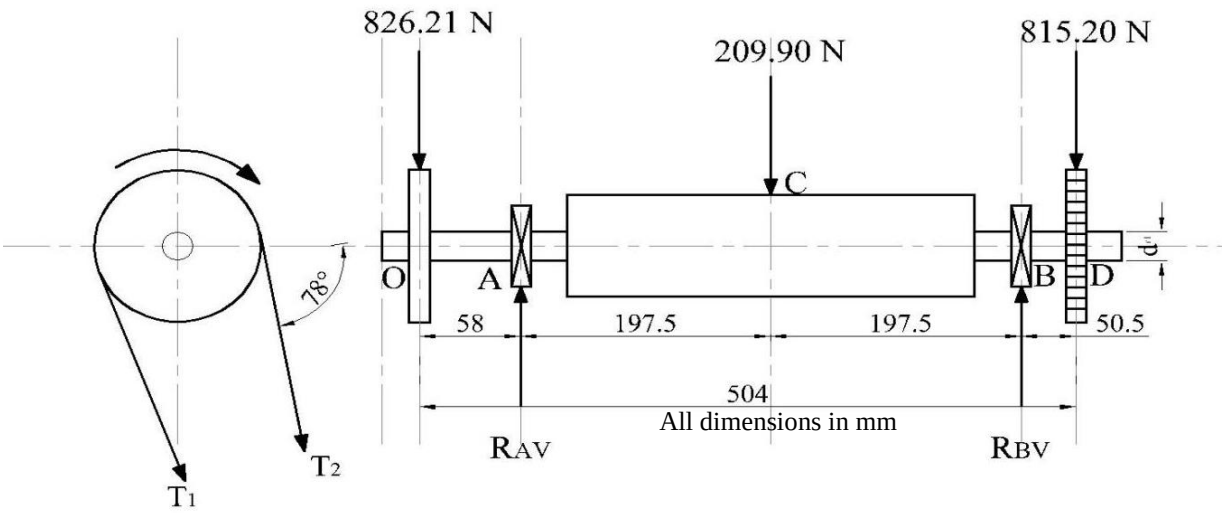

Figure 11. Load reactions on the roller-1 drive shaft due to vertical loading.

To determine R_{AV} and R_{BV}, equation 35 was adopted according to Khurmi and Gupta (2008).

$$\Sigma F_x = R_{AV} + R_{BV} = 1629.15$$

$$R_{AV} + R_{BV} = 1629.15\ N \quad (35)$$

Taking moment about R_{BV} in Figure 12.

$$R_{AV}(0.395) = 590.31(0.453) + 209.84(0.1975) - 829(0.0505) = 226.99\ N$$

$$R_{AV} = \frac{266.99}{0.395}$$

$$= 675.92\ N$$

From equation 35; $R_{AV} + R_{BV} = 1629.15\ N$

$$R_{BV} = 1629.15 - 675.92 = 953.23\ N$$

2.16.14. Bending moment at vertical loading

The bending moment on vertical loading, as shown in Figure 12 is calculated as follows:

$$BM_{OV} = 0\ Nm$$

$$BM_{AV} = -(590.31 \times 0.058) = -34.24\ Nm$$

$$BM_{CV} = -(590.31 \times 0.2555) + (675.92 \times 0.1975) = -17.33\ Nm$$

$$BM_{BV} = -(590.31 \times 0.453) + (675.92 \times 0.395) - (209.84 \times 0.1975) = -41.87\ Nm$$

$BM_{DV} = -(590.31 \times 0.5035) + (675.92 \times 0.4455) - (209.85 \times 0.248) + (953.23 \times 0.0505) = 0\ Nm$

Maximum bending moment due to vertical loading occurs at A, so

$$MBM_V = -41.87\ Nm$$

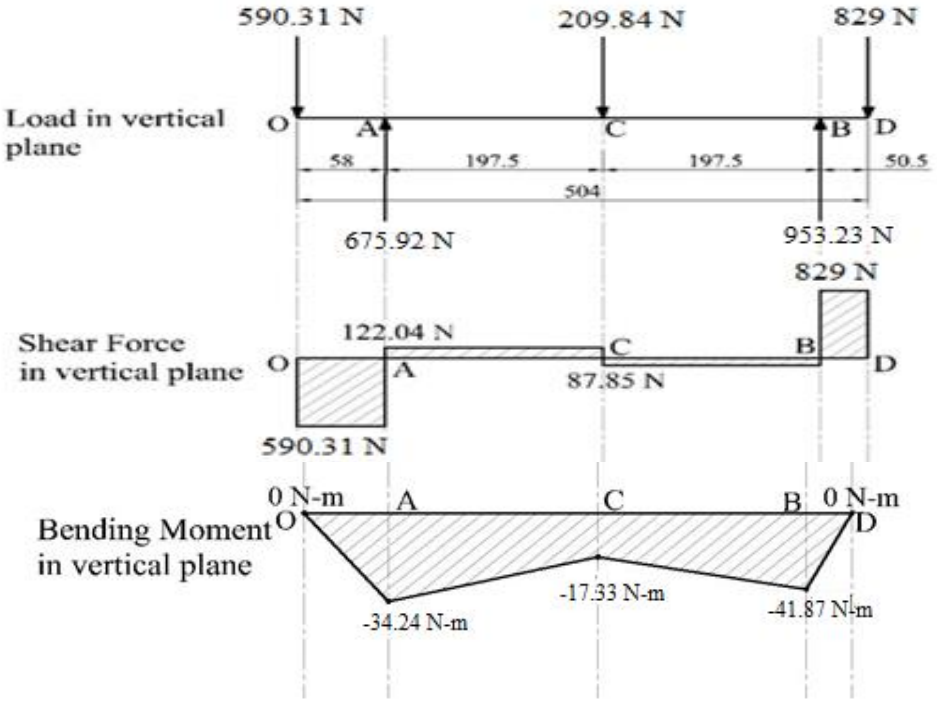

Figure 12. Shear force and bending moment diagram in the vertical plane for roller-1.

2.16.15. Reactions at the bearings due to horizontal loading

The reactions on the roller-1 shaft due to horizontal loading is shown in Figure 13.

To determine the reactions $R_{AH}$and R_{BH}, equation 36 was adopted according to Khurmi and Gupta (2008).

$$\Sigma F_x = R_{AH} + R_{BH} = 1171.4\ N$$

$$R_{AH} + R_{BH} = 1171.4\ N \quad (36)$$

Taking moment about R_{BH} in Figure 13.

$$R_{AH}(0.395) = 123.6(0.453) + 746.1(0.1975) - 301.7(0.0505) = 188.11\ N$$

$$R_{AH} = \frac{188.11}{0.395} = 476.23\ N$$

From equation 36; $R_{AH} + R_{BH} = 1171.40\ N$

$$R_{BH} = 1171.40 - 476.23 = 695.17\ N$$

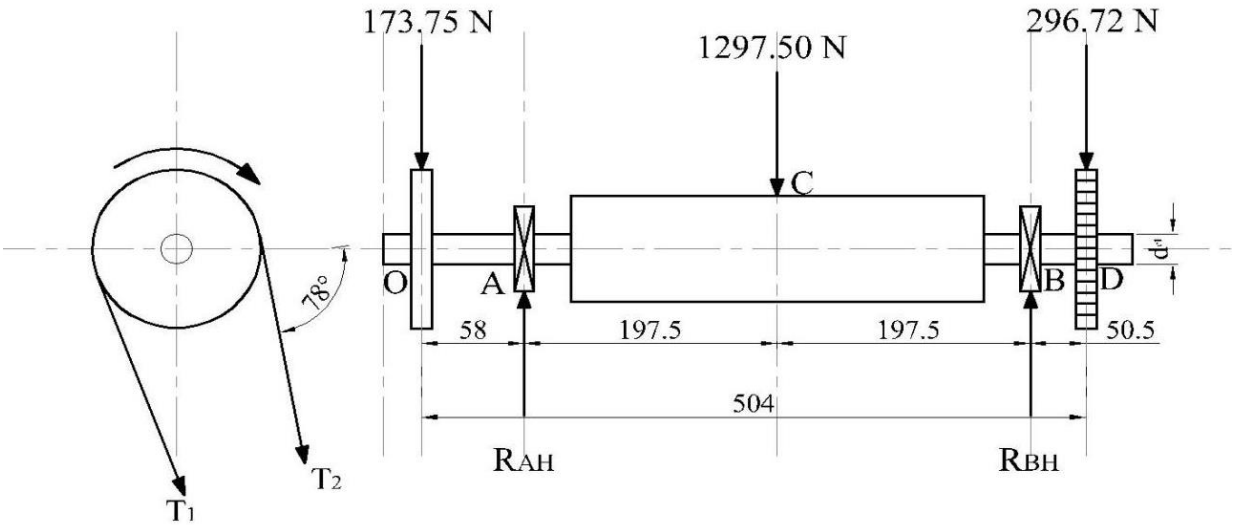

Figure 13. Load reactions on the roller-1 drive shaft due to horizontal loading.

2.16.17. Bending moment at horizontal loading

The bending moment on horizontal loading as shown in Figure 14 is calculated as follows

$$BM_{OH} = 0\ Nm$$
$$BM_{AH} = -(123.6 \times 0.058) = -7.17\ Nm$$
$$BM_{CH} = -(123.6 \times 0.2555) + (476.23 \times 0.1975) = 62.48\ Nm$$
$$BM_{BH} = -(123.6 \times 0.453) + (476.23 \times 0.395) - (746.10 \times 0.1975) = -15.23\ Nm$$
$$BM_{DH} = -(123.6 \times 0.5035) + (476.23 \times 0.4455) - (746.10 \times 0.248) + (695.17 \times 0.0505) = 0Nm$$

Maximum bending moment due to horizontal loading occurs at C, so

MBM_H = 62.48 Nm

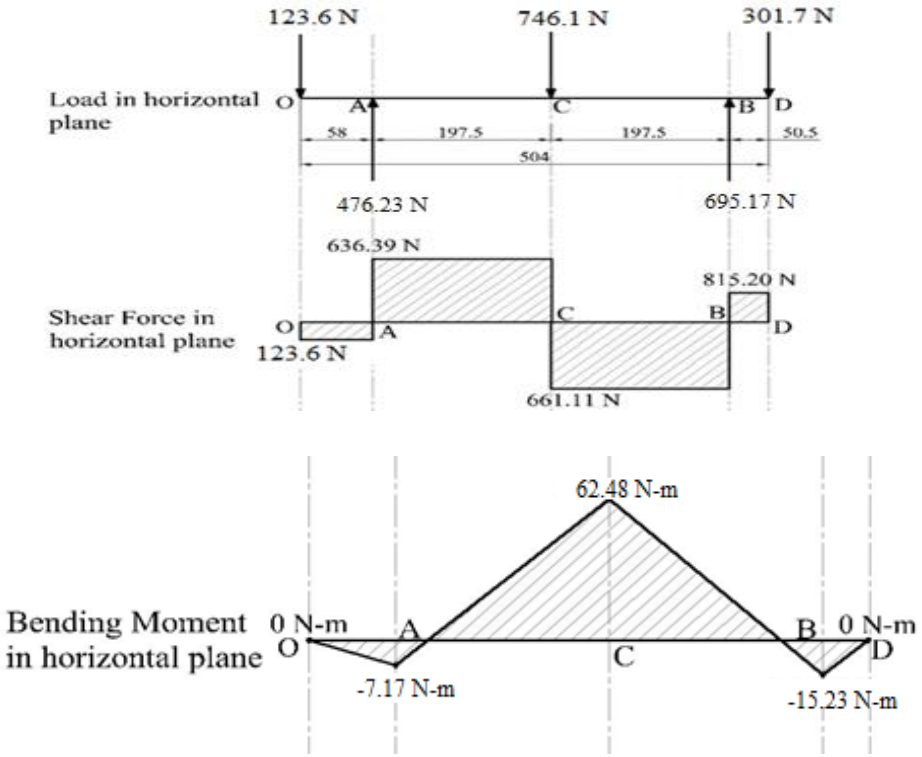

Figure 14. Shear force and bending moment diagram in the horizontal plane for roller-1.

2.16.18. Maximum bending moment (M_B)

The maximum bending moment, M_B on the roller-1 shaft was determined using Khurmi and Gupta (2008) expression given in equation 37.

$$M_B = \sqrt{MBM_V{}^2 + MBM_H{}^2} \quad (37)$$

where, MBM_V = maximum bending moment in the vertical plane,Nm;
MBM_H = maximum bending moment in the horizontal plane, Nm.
Therefore,

$$M_B = \sqrt{(-41.87)^2 + (62.48)^2} = 75.21\ Nm$$

2.16.19. Roller-1 shaft diameter (d_{r-1})

The shaft was designed for strength, rigidity and stiffness. The shaft was designed with the possibility of being subjected to twisting and bending moments.

The shaft diameter was determined based on A.S.M.E Code according to Collins et al. (2010); Fagbami et al. (2014); Shigley et al. (2011); Umani et al. (2020) utilizing equation 38 for shaft design as

$$d^3{}_{r-1}=\frac{16}{\pi\tau}\sqrt{M_B K_b{}^2 + M_T K_t{}^2} \quad (38)$$

where, τ = allowable shear stress brought on by bending and twisting, Nmm^{-2} = 56 MPa or 56 Nmm^{-2} for shaft without allowance for keyway; K_b= combined shock and fatigue factor applied to bending moment = 1.5 for minor shock; K_t = combined shock and fatigue factor applied to torsional moment = 1.5 for minor shock; M_B = maximum bending moment, $Nm = 75.21\ Nm$;M_T= torsional/twisting moment, Nm.

$M_T=\frac{P \times 60}{2\pi N_2} = \frac{1875.10 \times 60}{2\pi \times 160} = 111.91\ Nm$

Therefore, $d^3{}_{r-1}= \frac{16}{\pi \times 56 \times 10^6}\sqrt{1.5(75.21)^2 + 1.5(111.91)^2}$

$d^3{}_{r-1} = 0.00000009093\ (165.138) = 0.000015016;$

$d_{r-1} = 0.02467\ m = 24.67\ mm$

Therefore, the total shaft diameter is $24.67\ mm$.

However, $25\ mm$ shaft diameter was selected for the design of the roller-1 shaft. This provided for a safety factor of 1.0.

2.16.20. Design for roller-2 shaft

The roller-2 shaft was assessed to have less combined twisting and bending moments. However, a 25 mm shaft diameter was adopted. This was necessary to maintain mass balancing in order to reduce vibration tendencies.

2.16.21. Bearing selection for roller-1 and roller-2 shafts

Due to the high centrifugal force in roller shafts, the radial and thrust or axial loads on the two roller shafts are supported by two (2) deep groove ball bearings each. Deep groove ball bearing has comparatively high load-carrying capacity. It is designed to carry a radial, and it can also perform well under combined radial and axial loads (Harris & Rotzalas 2006).

According to Khurmi and Gupta (2008), the average life of a bearing is 5 times the rating or minimum life. Therefore, the bearing number 6204 having $10\ kN$ dynamic load capacity (for 25 mm and above shaft diameter at 62 series) was selected. The S-type bearings are used for highly contaminated environment, shaft deflection and misalignment. It is mostly applicable in agricultural machines, and conveyor systems (FAG Catalogue 2006).

2.17. Design of the frames

The frames were made of mild steel bars with a rectangular cross-section. The frames carried the weights of two periwinkle rollers, the electric motor, the gears, the pulley, and the hopper with periwinkles in it. The thickness of the frame was estimated using the procedure outlined by Umani et al. (2020) for the determination of the thickness of rectangular bars of known width. The equation 36 was used.

$$S_r = \frac{S_e}{F_s} - \frac{S_e}{S_{yp}} \times S_m \quad (39)$$

where S_r = superimposed alternating stress, , kNm^{-2}; S_e = maximum endurance stress of mild steel = $107.696 \times 10^3 kNm^{-2}$ (Etoamaihe & Iwe 2014)

S_{yp} = yield strength of mild steel = $801.414 \times 10^3\ kNm^{-2}$

S_m= mean stress

But,

$$S_r = \frac{\sigma_{max} - \sigma_{min}}{2} \quad (40)$$

$$S_m = \frac{\sigma_{max} + \sigma_{min}}{2} \quad (41)$$

where σ_{max} =maximum stress, kNm^{-2} and σ_{min} = minimum stress, kNm^{-2}

A mild steel angle bar of $3\ mm$ thickness with a $38\ mm$ width was selected for the machine in order to avoid under-estimation.

Note: The weight of the machine's components like the hopper, the shafts, electric motor, pulleys, and gears on the frame causes the minimum stress, while the maximum stress is owing to all the aforementioned weights plus the weight due to the periwinkles used in filling the hopper and the force applied by the electric motor on the machine members.

2.17.1. Bolts selection for the frames

To determine the bolt size for the frame, the shear stress induced on the bolt due to the weight of the machine was evaluated. According to Shigley et al. (2011), the bolt size was expressed as

$$S_e = \frac{F_{max}}{\pi d^2/4} \quad (42)$$

$$d = \sqrt{4F_{max}/\pi S_e} \quad (43)$$

where, S_e= allowable endurance stress of mild steel = $107.696 \times 10^3 kNm^{-2}$
$F_{max} = F_{min}$ + weight of periwinkles filling the hopper,
F_{min} = force due to total weight of the machine without load, (kN)
Thus, $d\ was\ computed\ to\ be = 0.010\ m = 10\ mm.$
Hence, 12 mm bolts were selected to fasten the machine to its frame.

2.18. Design of screen aperture

The screen aperture can be round, rectangular or oblong according to the width of the cracked periwinkle shell particles. The open area of square screen wire can be determined using the equation of Sahay and Singh (1994) presented by Ndirika and Onwualu (2016) given as

$$A_1 = \frac{\varphi^2}{(\varphi+D)^2} \times 100 \quad (44)$$

where A_1 = Open area (%) for screen one,φ = size of opening (mm),D = wire diameter (mm)

$$A_1 = \frac{10^2}{(10+2)^2} \times 100 = 69.4\%$$

$$A_1 = \frac{10^2}{(10+2)^2} \times 100 = 69.4\%$$

Where A_2 = Open area (%) for screen two

$$A_2 = \frac{\varphi^2}{(\varphi+D)^2} \times 100 = \frac{6^2}{(6+2)^2} \times 100 = 56.3\%$$

2.18.1. The capacity of screen (C_s)

The bigger the size of the holes of the screen, the better the efficiency, this was expressed by equation given by Igbeka (2013) as

$$C_s = K \times A \times a \quad (45)$$

where K = characteristic constant
A = Area of hole, m^2
a = width or diameter of hole (m)
For screen one
$C_{s1} = K \times A \times a = 0.25 \times 10 \times 10 \times 10 = 250\ mm^3$
For screen two
$C_{s2} = K \times A \times a = 0.25 \times 6 \times 6 \times 6 = 54\ mm^3$

2.19. Design of water supply system

The water supply system consisted of a variety of essential components such as a pressure source; a pump, and piping connections with valves to move water for cleaning the separated periwinkle meat as shown in Figure 15.

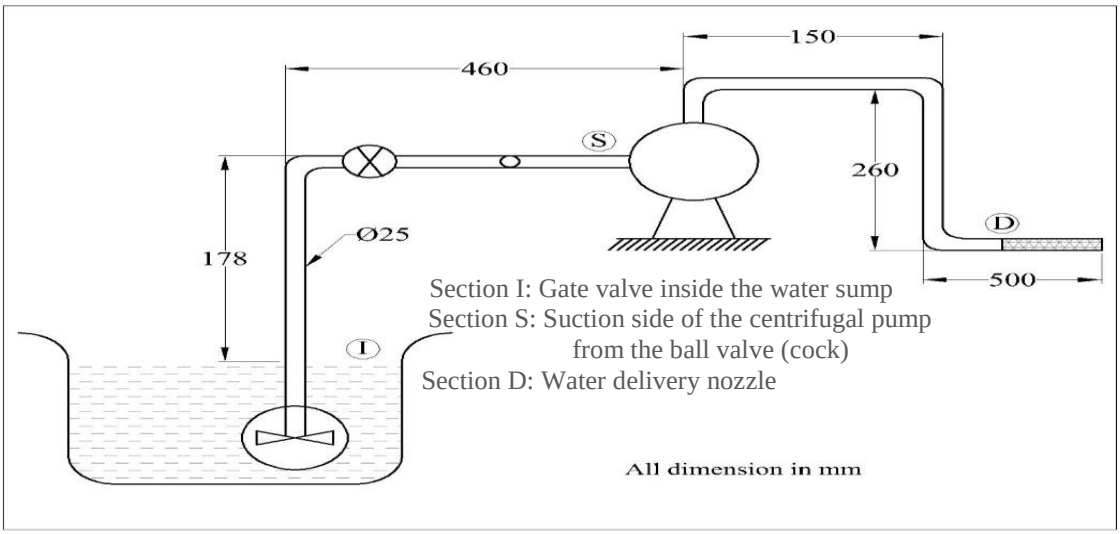

Figure 15. Schematic diagram of the water supply system.

2.19.1. Components of the water supply system

2.19.1.1. Pump

The pump is an important part of the water supply system, it transfers water from the tank through positive displacement action to the suction or intake port of the pump.

2.19.1.2. PVC pipe and control valves

Pipes are essential for the transportation of fluids (water) with the aid of pumps for various agricultural and food processing operations. The flow control valves helped in controlling the rate of flow of water within the system.

2.19.1.3. Pump sizing and selection

The power requirement of the pump depends on the amount of fluid (water) to be delivered. Centrifugal pump was chosen for the system. Neglecting all losses, the power output of the pump

$$P_c = wQH_T \quad (46)$$

As given by Rajput (2007)

Where $P_c = 0.5hp = 0.373kW(specified); Q =$ pump delivery, $\frac{17L}{\text{mins.}(specified)} = \frac{2.833\times10^{-4}m^3}{s}$;

$H_T =$ energy added by the pump per unit weightof water pumped(m); V_p = velocity of water in the pipe

$$V_P = {}^{Q}/_{A} \quad (47)$$

A = surface area of pipe $= {}^{\pi D^2}/_{4} = {}^{\pi \times 0.025^2}/_{4} = 4.909 \times 10^{-4}m$

$$V_P = \frac{\frac{2.833\times10^{-4}m^3}{s}}{4.909\times10^{-4}m} = 0.5771\, m/s$$

$P_c = wQH_T = 0.373kW\ hence\ H_T = 0.373 \times 10^3/9.81 \times 10^3 2.833 \times 10^{-4} = 134$m

Applying Bernoulli's equation to points I and D

$$P_1/w + {V^2}_1/2g + Z_1 + H_P = P_D/w + {V^2}_D/2g + Z_d \quad (48)$$

$$0 + 0 + 0 + 134 = P_D/w + 0.5771^2/2 \times 9.81 + 0.082$$

$$P_D/w = 133.9\, m; P_D = 1313.6kN/m^2$$

2.20. Working principle of the machine

The conditioned periwinkles are introduced into the running machine through the hopper where they flow down through a controlled feed gate opening to the revolving rollers for periwinkle shell cracking operation. The cracked periwinkle shells together with its meat fall into the reciprocating two-tier separating sieving screens equipped with a steady shower of water to clean the meats and dislodge any adhered shells. The separated meat flows through the trough and are collected while the shells fall directly below to the waste trough (Figure16).

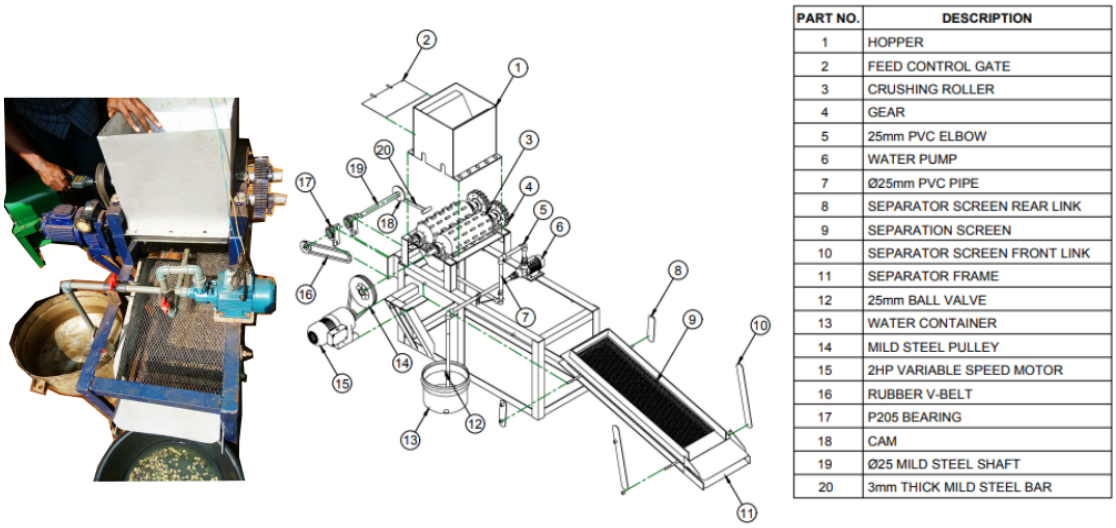

PART NO.	DESCRIPTION
1	HOPPER
2	FEED CONTROL GATE
3	CRUSHING ROLLER
4	GEAR
5	25mm PVC ELBOW
6	WATER PUMP
7	Ø25mm PVC PIPE
8	SEPARATOR SCREEN REAR LINK
9	SEPARATION SCREEN
10	SEPARATOR SCREEN FRONT LINK
11	SEPARATOR FRAME
12	25mm BALL VALVE
13	WATER CONTAINER
14	MILD STEEL PULLEY
15	2HP VARIABLE SPEED MOTOR
16	RUBBER V-BELT
17	P205 BEARING
18	CAM
19	Ø25 MILD STEEL SHAFT
20	3mm THICK MILD STEEL BAR

Figure 16. Exploded view of the periwinkle meat extraction machine

2.21. Performance Evaluation of developed periwinkle meat processing machine

Freshly harvested periwinkles were procured at a local water front market in Itu, Akwa Ibom State. The periwinkle samples were then cleaned manually to remove dirt and foreign materials, graded thereafter weighed using electronic weighing balance (Ohaus – Scout Pro) with an accuracy of 0.001g. The experiment was performed in triplicates as adopted by Ekop et al. (2021).

2.22. Design of experiment and statistical analysis

Measurements were replicated three times, and data were subjected to analysis of variance and main effects plots. The performance of the periwinkle processing machine was designed as a function of the machine operating parameters and crop factors: cracking speed (CS), agitating speed (AS), feed rate (FR), heat condition time (HCT) and the response variable(s) namely: the periwinkle cracking efficiency (CE), separating efficiency (SE), throughput (TP) and periwinkle meat loss (PML). Also, the obtained results of the experiment were analyzed as reported Ekop et al. (2021).

Table 2. The periwinkle machine performance at different processing conditions.

Runs Order	*CS* (rpm)	*FR* (kgs^{-1})	AS ($m\ s^{-1}$)	*HCT* (mins)	*CE* (%)	*SE* (%)	*TP* (kgh^{-1})	*PML* (%)
1	120	0.30	1.04	0	70.95	54.70	15.10	43.30
2	110	0.20	0.95	2	63.07	61.31	16.81	31.48
3	130	0.20	1.11	2	65.94	66.07	19.43	22.93
4	110	0.40	0.95	2	64.75	68.53	18.33	29.88
5	130	0.40	1.11	2	69.79	72.38	20.61	11.62
6	120	0.10	0.95	4	69.74	62.39	16.84	30.56
7	100	0.30	1.11	4	58.63	63.91	20.47	18.09
8	120	0.30	0.95	4	79.83	67.56	14.81	34.74
9	120	0.30	1.11	4	79.52	69.25	21.10	38.75
10	120	0.30	1.04	4	79.66	68.29	17.64	10.71
11	120	0.30	1.04	4	79.59	59.17	17.32	16.23
12	120	0.30	0.76	4	79.42	60.38	13.37	34.62
13	120	0.30	1.04	4	79.97	71.67	15.34	18.64
14	140	0.30	1.04	4	78.61	71.94	15.58	18.06
15	120	0.50	1.04	4	72.34	71.72	15.29	18.88
16	110	0.20	1.04	6	71.54	71.84	15.11	18.06
17	130	0.20	1.04	6	84.05	71.88	15.71	18.42
18	110	0.40	1.04	6	66.68	71.74	15.54	18.78
19	130	0.40	1.23	6	79.67	78.79	26.79	17.06
20	120	0.30	1.04	8	78.68	71.17	17.89	26.36

CS = Cracking Speed, *FR* = Feed Rate, AS = Agitating Speed, *HCT* = Heat Conditioning Time, *CE* = Cracking Efficiency, *SE* = Separating Efficiency, *TP* = Throughput, *PML* = Periwinkle Meat Loss.

3. RESULTS AND DISCUSSIONS

Table 2 presents the data obtained during performance operations of the developed machine. *CE* an essential machine response variable that entails the quantity of periwinkle cracked with respect to what was fed into the machine. The optimum *CE* was found to be 84.05% when periwinkle *HCT* was 6 min at *CS* of 130 rpm and *FR* of 0.20kg/s while the least *CE* of 58.63% was obtained when periwinkle *HCT* was 4 min at *CS* of 100 rpm and *FR* of 0.30kg/s (Ekop et al.,2021). There is information dart on periwinkle and related mollusk processing. However, Dixit and Ravindra (2022) obtained a machine cracking efficiency of 82.1% at 43 rpm for walnut while Hussain et al., (2018) obtained a shelling (cracking) efficiency of 96 % for walnut although machine parameters were not specifically mentioned.

The result for *SE* indicated that the most efficient separation can be achieved when *HCT*, *CS*, *AS* and *FR* at 6 min,130 rpm,1.11m/s and 0.40 kg/s respectively.*SE* gives the amount periwinkle separated based on the amount of periwinkle cracked. This was found to be 78.79% whereas its lowest *SE* of 54.70% was obtained when *HCT*, *CS*, *AS* and *FR* at 0 min,120 rpm,1.04 m/s and 0.30 kg/s. Although there is no related literature on periwinkle processing, but Akubuo and Eje (2002) working on palm kernel recorded an optimum *SE* to be 82.1% at 93/min crank speed.

The highest *TP* value of 26.79 kg/h was obtained when the machine was operated at *CS* of 130 rpm, *AS* of 1.23 m/s under the *HCT* of 6 min at *FR* of 0.40 kg/s while the lowest *TP* value of 13.37 kg/h was recorded at *CS* of 120 rpm, *AS* of 0.76 m/s, *FR* of 0.30 kg/s under the *HCT* of 4 min. *TP* shows the quantity of periwinkle meat separated per unit time. This is a unique in performance evaluation of the periwinkle machine. Accordingly, the lowest *PML* value of 10.71 % was obtained when the machine was operated at *CS* of 120 rpm, *AS* of 1.04 m/s under the *HCT* of 4 min at feed rate of 0.30 kg/s but the maximum *PML* value was recorded when the machine was operated at *CS* of 120 rpm, *AS* of 1.04 m/s, feed rate of 0.30 kg/s under the *HCT* of 0 min. There is no other research conducted in this domain for various processing conditions and machine parameters of periwinkle.

3.1. Effects of the cracking speed, feed rate and heat conditioning time on the periwinkle cracking efficiency

Figure 17(A) shows the relationship between the mean response (periwinkle cracking efficiency) and the different levels of machine operation parameters (cracking speed, feed rate) and crop factor (heat conditioning time). The reference line in the main effects plot is the overall mean for the response. It shows that cracking speeds of 120,130 and 140 rpm and feed rate of 0.3 kgs^{-1} and heat conditioning time of 4, 6 and 8 minutes are associated with the highest mean cracking efficiency. Hence, these combinations represent the best option for achieving optimum periwinkle cracking efficiency.

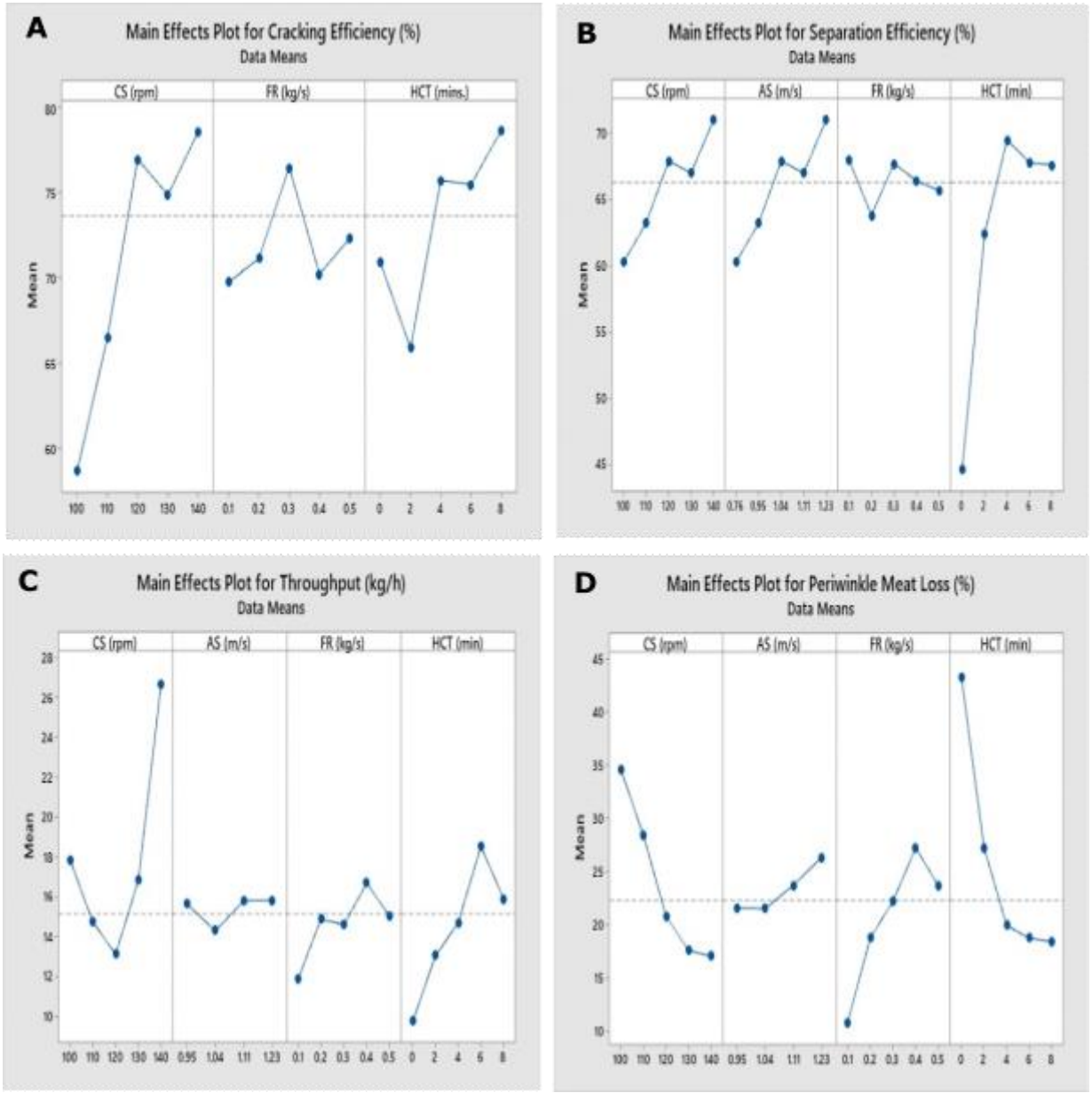

Figure 17 Main effects for:(**A**) periwinkle shell cracking efficiency, (**B**) periwinkle meat separating efficiency, (**C**) periwinkle meat throughput, (**D**) periwinkle meat loss.

The analysis of variance for the effects of cracking speed, feed rate, heat conditioning time on cracking efficiency is presented in supplementary table 1. The results indicate that the *p*-value for the cracking speed, feed rate and heating conditioning time are 0.0001, 0.015 and 0.0007 respectively. Since the *p*-values for the machine variables (cracking speed, feed rate, and heat conditioning time) are less than the chosen α-level of 0.05, it means that the effects of cracking speed, feed rate and heating conditioning time is statistically significant (Ekop et al., 2021).

3.2. Effects of the cracking speed, agitation speed, feed rate and heat conditioning time on the periwinkle separation efficiency

Figure 17(B) presents the relationship between the mean response (separation efficiency) between four levels of machine parameters and crop factor; cracking speed, agitation speed, feed rate and heat conditioning time. The reference line in the main effects plot is the overall mean for the response. It shows that cracking speed of 120,130 and 140 rpm, agitation speed of 1.04, 1.11 and 1.23 m/s and feed rate of 0.1 and 0.3 kg/s and heat condition time of 4, 6 and 8 minutes are associated with the highest mean separation efficiency. Thus, the best combinations for optimum periwinkle separation efficiency.

Analysis of variance for the effects of cracking speed, agitation speed, feed rate, heat conditioning time on separating efficiency is presented in supplementary table 2. The results indicate that the *p*-value for the cracking speed, agitation speed, feed rate and heat conditioning time are 0.0025,0.001,0.0409 and 0.0386 respectively. Since the *p*-values for the machine separation variables are less than the chosen α-level of 0.05, it means that the effects of cracking speed, agitation speed, feed rate and heating conditioning time is statistically significant (Ekop et al., 2023).

3.3. Effects of the cracking speed, agitation speed, feed rate and heat conditioning time on the periwinkle throughput

Figure 17(C) shows the relationship between the mean response (throughput) between four levels of machine parameters and crop factor; cracking speed, agitation speed, feed rate and heat conditioning time. This indicates that cracking speed of 100,130 and 140 rpm, agitation speed of 0.95, 1.11 and 1.23 m/s and feed rate of 0.4 and 0.5 kg/s and heat conditioning time of 6 and 8 minutes are associated with the highest mean throughput. Therefore, the best combination for optimum periwinkle meat throughput.

Also, analysis of variance for the effects of cracking speed, agitation speed, feed rate, heat conditioning time on throughput is presented in supplementary table 3. The results indicate that the *p*-value for the cracking speed, agitation speed, feed rate and heat conditioning time are 0.0140, 0.0466, 0.0182 and 0.0189 respectively. Since the *p*-value for cracking speed and heat conditioning time are less than the chosen α-level of 0.05, it means that the effects of the four machine operation parameters and crop factor are statistically significant.

3.4. Effects of the cracking speed, agitation speed, feed rate and heat conditioning time on the periwinkle meat loss

Figure 17(D) shows the relationship between the mean response (meat loss) between four levels of machine parameters and crop factor; cracking speed, agitation speed, feed rate and heat conditioning time. It entails that cracking speed of 100 and 110 rpm, agitation speed of 1.11 and 1.23 m/s and feed rate of 0.4 and 0.5 kg/s and heat condition time of 0 and 2 minutes are associated with the highest mean meat loss. Thus, combining these machine parameters give an optimum periwinkle meat loss but our aim is to minimize periwinkle meat loss as much as possible.

Analysis of variance for the effects of cracking speed, agitation speed, feed rate, heat conditioning time on periwinkle meat loss is presented in supplementary table 4. The results point out that the *p*-value for the cracking speed and agitation speed, feed rate and heat conditioning time are 0.0005, 0.8369, 0.0365 and 0.0013 respectively. Since the *p*-value for cracking speed, feed rate and heat conditioning time are less than the chosen α-level of 0.05, it means that the effects of cracking, feed rate and heat conditioning time are statistically significant.

4. CONCLUSION

The periwinkle machine meat processing machine was designed, developed, and evaluated based on the essential data available for physical, mechanical and thermal properties of the periwinkle. It was established that processing factors and crop condition influence the periwinkle meat cracking efficiency, separation efficiency, throughput and meat loss. The developed periwinkle meat processing machine serves as a viable option for periwinkle meat processors in that it would efficiency replaced the time-consuming, crude manual method that often times help add contaminants to the meat. With the availability of machine for periwinkle meat processing, economic potentials of periwinkle meat become more realistic.

CONFLICTS OF INTEREST

The authors declare no conflict of interest regarding this work.

AUTHORS' CONTRIBUTIONS

Authors equally contributed to this work.

REFERENCES

Akubuo, C., & Eje, B. E. (2002). PH-Postharvest technology: Palm kernel and shell separator. *Bioresources Engineering*, 81(2),193-199.

Collins, J. A., Busby, H. R., & Staab, G. H. (2010). Mechanical design of machine elements and machines: failure preventive perspective. US: John Wiley & Sons, Inc.

Dixit, J., & Ravindra, K. (2022). Design and development of walnut cracking machine. *Agricultural Engineering International: CIGR Journal*, 24(4),143-152.

Ekop, I. E., Simonyan, K. J., & Onwuka, U.N. (2019). Comparative analysis of thermal properties of two varieties of periwinkle relevant to its processing equipment design. *American Journal Food Science and Technology*,7(6),189-194. https://doi.org/10.12691/ajfst-7-6-4

Ekop, I. E., Simonyan, K. J., & Onwuka, U.N. (2021). Effects of processing factors and conditions on the cracking efficiency of *Tympanotonus fuscatus* and *Pachymelania aurita* periwinkles: Response surface approach. *Journal Agriculture and Food Research*, 3(3),1-7. https://doi.org/10.1016/j.jafr.2020.100094

Ekop, I. E., Simonyan, K. J., & Onwuka, U. N. (2022). Comparative analysis of mechanical properties of two varieties of periwinkle relevant to its processing equipment design. *Agricultural Engineering International: CIGR Journal*, 24(2),122-136.

Ekop, I. E., Simonyan, K. J., Onwuka, U. N. & Ekop, I. E (2023). Optimization of processing machine parameters for separating efficiency of periwinkles. *Journal of Aquatic Food Product Technology*.33(1),98-110 https://doi.org/10.1080/10498850.2023.2291371

Etoamaihe, U. J., & Iwe, M. O. (2014). Development and performance evaluation of a reciprocating motion cassava shredder. *International Journal of Engineering Science*, 3(4),6-15.

FAG Catalogue WL 41520EA (2006). *Rolling bearing*. https://www.ahrinternational.com/PDF_catalogues (pp. 9-15).

Fagbami, E. A., Okeeseni, A., Omonigho, B., Iseru, E., Akpovwovwo, T., & Awolola, E.K. (2014). Forms and design analysis of mechanical shafts used in agricultural machineries. *International Journal of Agricultural Science and Natural Resources*, 1(5),103-106.

Harris, T. A., & Rotzalas, M. N. (2006). Essential concept of bearing technology. *Rolling Bearing Analysis*, 5th Ed., CRC press. Taylor and Francis Group,NY.

Hicks, T. G. (2004). *Standard handbook of engineering calculations*. McGraw-Hill. https://www.pdfdrive.com/standard handbook of engineering calculations

Hussain, S. Z., Ammatullah, B., Kanojia, V., Reshi, M., Naseer, B., & Naik, H. R. (2018). Design and development of technology for walnut cracking. *Journal of Food Science and Technology*, 55(12),4973-4983.

Igbeka, J. C. (2013). *Agricultural processing and storage engineering*. Ibadan University Press.53.

Jamabo, N., & Chinda, A. (2010). Aspects of the ecology of *Tympanotonus fuscatus var fuscatus* (Linnaeus, 1758) in the mangrove swamps of the upper Bonny River, Niger Delta, Nigeria. *Current Research Journal of Biological Science*, 2(1),42-7.

Khurmi, R. S., & Gupta, J. K. (2008). *A textbook of machine design*. (pp. 678-738). S. Chand publishing.

Mmom, P. C., & Arokoyu, S. B. (2010). Mangrove forest depletion, biodiversity loss and traditional resources management practices in the Niger Delta, Nigeria. *Research Journal of Applied Science, Engineering and Technology*, 2(1),28-34.

Ndirika, V. I. O., & Onwualu, A. P. (2016). *Design principles for post-harvest machines*, First edition. (pp.126-131). Naphtali Print, Nigeria.

Odu, N. N., Obafemi, A., & Njoku, H.O. (2010). Comparative assessment of bacteriological quality and proximate composition of laboratory shucked and traditionally shucked tropical periwinkle (*Tympanotonus fuscatus*), *Scientia Africana*, 9(1),140-9.

Otto, H. (2015). *New general mathematics for secondary senior schools 1*, (pp. 43-44). Pearson Edu Ltd, Eng.

Rajput, R. K. (2007). *A textbook of fluid mechanics and hydraulic machines*. 6th Ed. (pp.280-291) S. Chand.

Sahay, K. M., & Singh, R. K. (1994). *Unit operations of agricultural process*, (pp. 65-74). Vikas Publishing House PVT Ltd.

Shigley, J. E., Mischke, C. R., Budnyas, R. G., & Nisbett, K. J. (2011). *Shigley's mechanical engineering design* (SI Units), (Sie). Tata McGraw-Hill. https://ia903102.us.archive.org.

Umani, K. C., Fakayode, O. A., Ituen, E. U., & Okokon, F. B. (2019). Development and testing of an automated contact plate unit for a cassava grater. *Computers and electronics in agriculture*, *157*, 530-540.

Umani, K. C., Ituen, E. U. U., & Fakayode, O. A. (2020). Development and testing of a double-action cassava grater with an automated contact plate. *Journal of Food Process Engineering*. https://doi.org/10.1111/jfpe.13372

V-Belt Design Manual (2017). *The right belt for all applications* 2017. https://www.bandousa.com